Anal. Chem. **2009,** *81,* 618–624

Ion Mobility-Mass Spectrometer Interface for Collisional Activation of Mobility Separated Ions

Francisco A. Fernandez-Lima, Christopher Becker, Kent J. Gillig, William K. Russell, Shane E. Tichy, and David H. Russell*

Department of Chemistry, Texas A&M University, College Station, Texas 77843

An ion mobility-mass spectrometer (IM-MS) interface is described that can be employed to perform collisional activation and/or collision-induced dissociation (CID) with good transmission of mobility separated ions to the MS analyzer. The IM-MS interface consists of a stacked-ring ion guide design, where the field strength and pressure ratio can be operated such that structural rearrangement reactions and/or CID are achieved as a function of the effective ion temperature. The ion dynamics and collisional activation processes in the IM-MS interface are described as a function of the ion-neutral collisions, ion kinetic energies, and effective ion temperature. The applicability of the IM-CID-MS methodology to studies of peptide ion fragmentation is illustrated using a series of model peptides.

Since the introduction of electrospray ionization (ESI) and matrix-assisted laser desorption/ionization (MALDI), there has been explosive growth in the area of biological mass spectrometry.[1−4] Biological mass spectrometry has also benefited greatly from technological advances in time-of-flight mass spectrometry (TOF-MS), as well as instrumentation specifically designed for acquisition of fragment ion spectra, namely, post-source decay (PSD)[5−7] and tandem MS instruments.[8−17] MALDI and TOF-MS are highly compatible and the analytical utility of MALDI-TOF-MS has been further complimented by advances in off-line high performance liquid chromatography (HPLC) and capillary electrophoresis (CE) for high throughput peptide sequencing and tandem MS experiments for interrogation of complex chemical mixtures, that is, characterization and identification of peptides and proteins using enzymatic digestion.[18−23]

Tandem MS has proven to be an effective method for elucidating molecular structure, especially for the analysis of biological compounds. A drawback of tandem TOF-MS for complex mixture analysis is the requirement for serial data acquisition. That is, ions are preselected by MS^1, subjected to collisional activation, and the resulting fragment ion spectra (MS^2) are recorded and stored.[24−26] To achieve a higher throughput in the tandem MS analysis, several research groups have attempted to design instruments and data acquisition techniques that circumvent serial data acquisition.[27−32] In particular, we have previously demonstrated that IM-MS can be used for acquisition of fragment ion spectra data without preselecting the parent ions since they are already separated in the IM domain.[33,34] Further improvement in ion transmission and fragmentation efficiencies of IM-MS instrumentation is needed.

* To whom correspondence should be addressed. E-mail: russell@mail.chem.tamu.edu.

(1) Whitehouse, C. M.; Dreyer, R. N.; Yamashita, M.; Fenn, J. B. *Anal. Chem.* **1985**, *57*, 675–679.
(2) Cole, R. B. *Electrospray Ionization Mass Spectrometry*; John Wiley & Sons: New York, 1997.
(3) Karas, M.; Bachmann, D.; Hillenkamp, F. *Anal. Chem.* **1985**, *57*, 2935–2939.
(4) Hillenkamp, F.; Karas, M. *Int. J. Mass Spectrom.* **2000**, *200*, 71–77.
(5) Spengler, B.; Kirsch, D.; Kaufmann, R.; Lemoine, J. *Org. Mass Spectrom.* **1994**, *29*, 782–787.
(6) Hoffmann, R.; Metzger, S.; Spengler, B., Jr. *J. Mass Spectrom.* **1999**, *34*, 1195–1204.
(7) Fournier, I.; Chaurand, P.; Bolbach, G.; Lützenkirchen, F.; Spengler, B.; Tabet, J. C. *J. Mass Spectrom.* **2000**, *35*, 1425–1433.
(8) Schey, K. L.; Graham Cooks, R.; Kraft, A.; Grix, R.; Wollnik, H. *Int. J. Mass Spectrom. Ion Processes* **1989**, *94*, 1–14.
(9) Boesl, U.; Weinkauf, R.; Schlag, E. W. *Int. J. Mass Spectrom. Ion Processes* **1992**, *112*, 121–166.
(10) Daniel, R.; Jardine; Morgan, J.; Alderdice, D. S.; Derrick, P. J. *Org. Mass Spectrom.* **1992**, *27*, 1077–1083.
(11) Cornish, T. J.; Cotter, R. J. *Anal. Chem.* **1993**, *65*, 1043–1047.
(12) Seeterlin, M. A.; Vlasak, P. R.; Beussman, D. J.; McLane, R. D.; Enke, C. G. *J. Am. Soc. Mass Spectrom.* **1993**, *4*, 751–754.
(13) Strobel, F. H.; Russell, D. H. *ACS Symp. Ser.* **1994**, *549*, 73–94.
(14) Cornelis, E. C.; Hop, A. *J. Mass Spectrom.* **1998**, *33*, 397–398.
(15) Vestal, M.; Juhasz, P.; Hines, W.; Martin, S. *Mass Spectrom. Biol. Med.* **2000**, 1–16.
(16) Anastassios, E. G.; Benjamin, T.; Alex, W. C.; David, J. R.; Emmanuel, N. R.; Alexander, A. M.; Peter, J. D. *Rev. Sci. Instrum.* **2002**, *73*, 2115–2123.
(17) Vestal, M. *Abstracts of Papers*, 229th ACS National Meeting, San Diego, CA, U.S.A., 2005; ANYL-373.
(18) Williams, B. J.; Russell, W. K.; Russell, D. H. *Anal. Chem.* **2007**, *79*, 3850–3855.
(19) Rosas-Acosta, G.; Russell, W. K.; Deyrieux, A.; Russell, D. H.; Wilson, V. G. *Mol. Cell Proteomics* **2005**, *4*, 56–72.
(20) Wall, D. B.; Berger, S. J.; Finch, J. W.; Cohen, S. A.; Richardson, K.; Chapman, R.; Drabble, D.; Brown, J.; Gostick, D. *Electrophoresis* **2002**, *23*, 3193–3204.
(21) Johnson, T.; Bergquist, J.; Ekman, R.; Nordhoff, E.; Schurenberg, M.; Kloppel, K. D.; Muller, M.; Lehrach, H.; Gobom, J. *Anal. Chem.* **2001**, *73*, 1670–1675.
(22) Walker, K. L.; Chiu, R. W.; Monnig, C. A.; Wilkins, C. L. *Anal. Chem.* **1995**, *67*, 4197–4204.
(23) Nagra, D. S.; Li, L. *J. Chromatogr. A* **1995**, *711*, 235–245.
(24) Aebersold, R.; Goodlett, D. R. *Chem. Rev.* **2001**, *101*, 269–296.
(25) Larsen, M. R.; Roepstorff, P. *Fresenius' J. Anal. Chem.* **2000**, *366*, 677–690.
(26) Yates, J. R., III. *J. Mass Spectrom.* **1998**, *33*, 1–19.
(27) Enke, C. G.; Stults, J. T.; Holland, J. F.; Pinkston, J. D.; Allison, J.; Watson, J. T. *Int. J. Mass Spectrom. Ion Phys.* **1983**, *46*, 229–232.
(28) Stults, J. T.; Enke, C. G.; Holland, J. F. *Anal. Chem.* **1983**, *55*, 1323–1330.
(29) Russell, S. C.; Czerwieniec, G.; Lebrilla, C.; Steele, P.; Riot, V.; Coffee, K.; Frank, M.; Gard, E. E. *Anal. Chem.* **2005**, *77*, 4734–4741.
(30) Verentchikov, A. N.; Yavor, M. I.; Hasin, Y. I.; Gavrik, M. A. *Tech. Phys.* **2005**, *50*, 73–81.

10.1021/ac801919n CCC: $40.75
Published on Web 12/15/2008

In this work, we focus on the ion dynamic description of the CID process that is performed in the IM-MS interface as a way to obtain fragment ion spectra, that is, the collisional activation of parent ions is described. Ion dynamic simulations (i.e., number of ion-neutral collisions, ion kinetic energies, and effective ion temperatures) are presented and compared with experimental results. The application of a MALDI-IM-CID-MS platform is illustrated using a series of model peptides.

INSTRUMENTAL SECTION

The MALDI-IM-oTOF mass spectrometer used for these studies has been described previously.[35−39] Briefly, ions are formed in a IM drift cell by irradiating the sample plate with the output from a microcrystal Nd:YAG laser (355 nm, Powerchip Nanolaser, JDS Uniphase Corp.). In the IM drift cell, ions are separated on the basis of ion-neutral collision cross-sections; typical operating conditions are 3 torr of Helium buffer gas and field strength/pressure ratios (E/P) of 10−35 V cm^{-1} torr^{-1}. The IM drift cell consists of a stacked-ring ion guide design,[36,39] where electrode pairs are spaced 1.5 mm apart and the spacing between the electrode pairs is 3.0 mm. Subsequent electrodes are connected via a resistor divider network composed of 1 MΩ resistors. Thus, the field strength across electrode pairs is ΔV/1.5 mm, whereas the field strength between electrode pairs is ΔV/3.0 mm. This configuration yields an alternating high and low electric field strength for the stacked-ring ion guide design (Figure 1).[36] Note that the stacked-ring ion guide design[36,39] differs from the periodic focusing ion guide,[40,41] that is, the periodic focusing ion guide consists of thick, uniformly spaced ring electrodes, where the high and low field strength configuration is a consequence of the field strength between the electrodes and the penetrating electric field into the electrode's aperture, respectively.

For the study described here, the instrument was modified to allow the IM drift cell to operate as two independent cells (see Figure 1). Analogous to region 1, region 2 consists of a stacked-ring ion guide design,[36,39] where electrode pairs are spaced 1.5 mm apart and the spacing between the electrode pairs is 2.5 mm. Region 1 performs as a typical IM drift cell and achieves ion separation on the basis of ion neutral collision-cross section, and

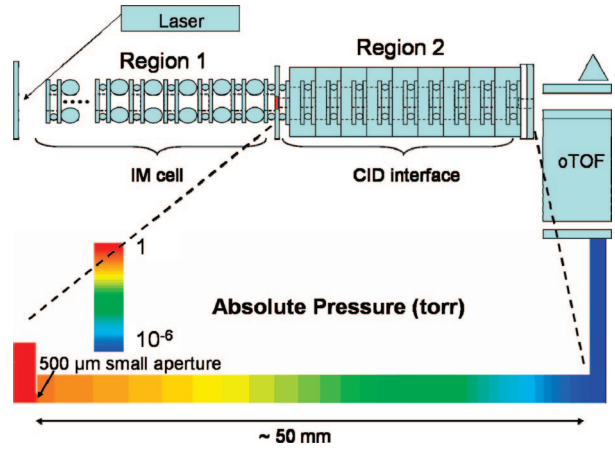

Figure 1. Schematic drawing of the IM-CID-oTOF instrument (Configuration **C**) and pressure drop (in color bar scales). The pressures in the IM cell and in the oTOF regions were set to 1 and 10^{-6} torr, respectively.

CID is performed in region 2. For example, the field strength (E) and pressure (P) applied to region 1 (IM drift cell), expressed as E/P ratio in units of V cm^{-1} torr^{-1}, was maintained in the range of 10−35 (low-field limit[42]); whereas in region 2, the E was tuned either to (i) a low-field value (e.g., ΔV = 90−135 V across 4.5 cm) to solely transfer the parent ions to the o-TOF, or (ii) a high-field value above the threshold for collisional activation (e.g., ΔV = 135−600 V across 4.5 cm) to induce dissociation and transfer the parent and fragment ions into the o-TOF source (Figure 1).

The ion source (MALDI sample plate) and IM drift cell is designed in such a way that gas admitted to the ion source leaks into the IM drift cell through a large diameter orifice (~3 mm, defined by the electrode inner diameters). Gas leaks through a smaller aperture (0.5 mm) into region 2 (CID region) and exits through a relatively large diameter orifice (~1.3 mm, defined by the electrode inner diameters). Thus, the pressure in region 1 (IM drift cell) is nearly constant, but the gas flow from region 1 through region 2 (CID region) into vacuum (10^{-5}−10^{-6} torr) produces a significant pressure gradient. In region 2, the increasing E/P ratio results in ion heating (collisional activation), which can result in rearrangement reactions and/or CID.

Ions exiting the IM drift cell are focused (by a multielement Einzel lens) into the o-TOF ion source. The TOF is biased at a potential of −6 kV, and the ions are extracted by applying a voltage pulse to the TOF push/pull electrodes (+675V/−675 V, respectively); the TOF extraction potential is pulsed at a rate 10−20 kHz, and typical mass resolution for the reflectron TOF is 3000. For comparison purposes, MS/MS and MS^n CID experiments were also performed in an Applied Biosystems 4700 Mass Spectrometer (Framingham, MA) and in a ThermoFinnigan LCQ Deca Mass Spectrometer (San Jose, CA), respectively.

ION TEMPERATURE SIMULATIONS

To understand the extent of ion heating that occurs in the IM-MS interface, we first modeled the pressure gradient using the

(31) Hoaglund-Hyzer, C. S.; Lee, Y. J.; Counterman, A. E.; Clemmer, D. E. *Anal. Chem.* **2002**, *74*, 992–1006.
(32) Valentine, S. J.; Koeniger, S. L.; Clemmer, D. E. *Anal. Chem.* **2003**, *75*, 6202–6208.
(33) Stone, E. G.; Gillig, K. J.; Ruotolo, B. T.; Russell, D. H. *Int. J. Mass Spectrom.* **2001**, *212*, 519–533.
(34) Sun, W.; May, J. C.; Russell, D. H. *Int. J. Mass Spectrom.* **2007**, *259*, 79–86.
(35) Koomen, J. M.; Ruotolo, B. T.; Gillig, K. J.; McLean, J. A.; Russell, D. H.; Kang, M.; Dunbar, K. R.; Fuhrer, K.; Gonin, M.; Schultz, J. A. *Anal. Bioanal. Chem.* **2002**, *373*, 612–617.
(36) Fuhrer, K.; Gonin, M.; Schultz, J. A. U.S. Patent Application Publ. US20050189486, 2005, p 38.
(37) Raznikov, V. V.; Schultz, J. A.; Egan, T. F.; Ugarov, M. V.; Tempez, A.; Savenkov, G.; Zelenov, V. In *Patent Cooperation Treaty Int. Appl. WO2006130475*; Ionwerks, Inc.: USA, 2006; p 73.
(38) Gillig, K. J.; Ruotolo, B.; Stone, E. G.; Russell, D. H.; Fuhrer, K.; Gonin, M.; Schultz, A. J. *Anal. Chem.* **2000**, *72*, 3965–3971.
(39) Schultz, J. A.; Raznikov, V.; Egan, T. F.; Ugarov, M. V.; Tempez, A. U.S. Patent Application Publ. US007223969B2, 2007, p 41.
(40) Gillig, K. J.; Ruotolo, B. T.; Stone, E. G.; Russell, D. H. *Int. J. Mass Spectrom.* **2004**, *239*, 43–49.
(41) Gillig, K. J.; Russell, D. H. In *Patent Cooperation Treaty Int. Appl. WO0165589*; Texas A & M University: College Station, TX, 2001; pp 36.
(42) Verbeck, G. F.; Ruotolo, B. T.; Gillig, K. J.; Russell, D. H. *J. Am. Soc. Mass Spectrom.* **2004**, *15*, 1320–1324.

Fluent 6.2.16 (Fluent, Inc., Lebanon, NH) computer software.[43] The pressure profile was incorporated into a Simion 3D[44] user developed program, which was used to determine the effective ion temperature (T_{eff}) along the interface axis. For these simulations, we assumed ideal gas behavior where the specific heat capacity (c_p), thermal conductivity, and viscosity parameters are determined by a Helium−Helium pair interaction potential (kinetic theory). A Helium−Helium Lennard−Jones potential with 2.96 Å equilibrium internuclear distance and 10.98 K interaction energy (ε/k) was employed.[45] The ion trajectories in region 1 and 2 were calculated considering an Elastic Hard Sphere Scattering model (EHSS) for the ion-Helium collisions.[46] Ion kinetic energy (KE) and number of collisions were recorded as a function of the distance along the axis of regions 1 and 2. The effective ion temperature (T_{eff}) was defined as the fraction (α) of the difference of the ion kinetic energy before (KE_i) and after the collision (KE_f) relative to the bath gas temperature (T_{BG}), that is, $T_{eff} = T_{BG} + \alpha(KE_i - KE_f)$. The α coefficient is typically determined from direct measurements of monatomic kinetic energies [47,48] or from the kinetics of reactions whose temperature dependence has been established by other means.[49−52] In this paper, we focus on the description of the ion dynamics rather than the absolute determination of T_{eff}, and we arbitrarily chose an alpha value of 0.5, which is a reasonable estimate for the ion kinetic energy difference (before and after collision) that can be converted to internal energy per collision.[53] Absolute determination of T_{eff} using this experimental setup will be discussed in a future paper.[54]

SAMPLE PREPARATION

The peptides used in this study were either purchased from Bachem Americas Inc., (Torrance, CA) (GGR, RGG, and GRG) or synthesized in our laboratory (WAGLK, RVGVAGG, VGVRAGG, and VGVAGGR). MALDI samples were prepared using a 1:1 matrix/analyte solution, which was then deposited on a stainless steel sample plate. The analyte concentration was 1 mg/mL in aqueous solution. Matrix solution was 5 mg/mL of α-Cyano-4-hydroxycinnamic (α-CHCA) in a mixture of acetonitrile/water (1:1 v/v) with final concentration of 0.1% of trifluoroacetic acid and 10 mM of ammonium phosphate. For MS^n experiments, peptides were electro-sprayed, at a concentration of 5 μmolar in a 1:1 (v/v) water/methanol with 1% acetic acid solution into a ThermoFinnigan LCQ Deca Mass Spectrometer.

(43) *Fluent*, 6.2.16 ed.; Fluent Inc.: Lebanon, NH.
(44) Scientific Instrument Services Inc.: Ringoes, NJ.
(45) Anderson, J. B. *J. Chem. Phys.* **2001**, *115*, 4546–4548.
(46) Ding, L.; Sudakov, M.; Kumashiro, S. *Int. J. Mass Spectrom.* **2002**, *221*, 117–138.
(47) Lunney, M. D. N.; Buchinger, F.; Moore, R. B. *J. Mod. Opt.* **1992**, *39*, 349–360.
(48) Vedel, F. *Int. J. Mass Spectrom. Ion Processes* **1991**, *106*, 33–61.
(49) Basic, C.; Eyler, J. R.; Yost, R. A. *J. Am. Soc. Mass Spectrom.* **1992**, *3*, 716–726.
(50) Brodbelt-Lustig, J. S.; Cooks, R. G. *Talanta* **1989**, *36*, 255–260.
(51) Hart, K. J.; McLuckey, S. A. *J. Am. Soc. Mass Spectrom.* **1994**, *5*, 250–259.
(52) Nourse, B. D.; Kenttamaa, H. I. *J. Phys. Chem.* **1990**, *94*, 5809–5812.
(53) Douglas, D. J. *J. Am. Soc. Mass Spectrom.* **1998**, *9*, 101–113.
(54) Fernandez-Lima, F. A.; Wei, H.; Gao, Y. Q.; Russel, D. H. *J. Phys. Chem. A* **2008**, submitted for publication.

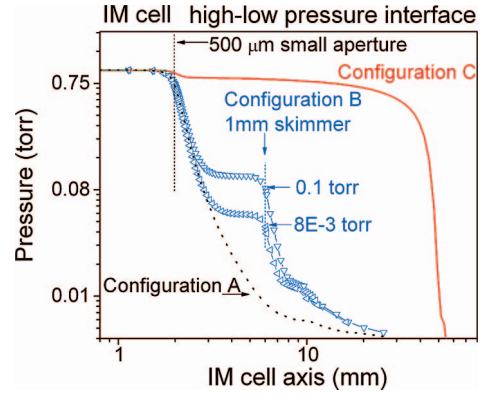

Figure 2. Calculated pressure gradient for three different interface configurations: (**A**) 500 μm aperture positioned at the exit of the drift cell, (**B**) 500 μm aperture followed by a 1 mm diameter skimmer positioned 4 mm downstream, and (**C**) a two compartment drift cell as shown in Figure 1. In each case the drift cell pressure is maintained at 1 torr of Helium and the TOF source at 10^{-6} torr. For **B**, plots are shown for two different pressures, 8×10^{-3} and 0.1 torr.

RESULTS AND DISCUSSION

The coupling of IM and TOF instruments involves the technical challenge of optimizing ion transmission from high pressure (1−10 torr; optimum pressure of the IM drift cell) to high vacuum regions ($10^{-6} - 10^{-8}$ torr; working pressure range of the TOF region) of the spectrometer. There are numerous ways to transfer ions from a high pressure to high vacuum region, but each design has specific advantages and disadvantages. For example, our original IM drift cell terminated to high vacuum using a small aperture (500 μm diameter). The sharp pressure drop on the low pressure side of the cell is ideal for most IM-TOF MS experiments[38] (pressure profile **A** in Figure 2), because the ions exiting the drift cell experience very few collisions which increases ion transmission to the TOF ion source. On the other hand, positioning a skimmer some distance (~4 mm) from the aperture (500 μm diameter) introduces a pressure plateau between the aperture and skimmer (pressure profile **B** in Figure 2). The pressure profile **B** is determined by the inner diameter of the skimmer and the background pressure in the aperture-skimmer region; characteristic pressure profiles for a 1 mm skimmer and a 8×10^{-3} and 10^{-1} torr pressure in the aperture-skimmer region are illustrated in Figure 2. Configuration **B** has the advantage of creating a differential pumping region and can be used for collisional heating, that is, declustering of ions and access to other low activation-energy fragmentation channels, by varying the field strength applied between the aperture and the skimmer. As described in this paper, a stacked-ring ion guide interface positioned after the IM cell expands the length of the higher pressure region (pressure profile **C** in Figure 2) and, analogous to configuration **B**, can be used for collisional activation. The main difference between the configuration **C** compared to **B** arises from the use of relatively lower electric field values to achieve the same ion heating conditions because of a higher number of ion-neutral collisions over the same distance, that is, the collisional activation regime is achieved in a more gentle way (low energy collisions) and the activation time is longer (~10−100 μs). In configuration **C**, once the parent ions achieve the collisional activation threshold, the excess and spread in kinetic energy of the fragment ions is smaller, and a higher ion transmission into

the o-TOF source is obtained relative to configuration **B**. The collisional activation in region 2 with a longer-length, high pressure region (configuration **C**) shares many similarities with early work done by Price et al. and Blom and Munson[55,56] where the extent of fragmentation in a drift-tube region at a 0.1−1.0 torr pressure was controlled by the drift voltage setting.

The pressure drop in an IM-MS interface is defined by the pressure difference in the IM and TOF region, the pumping speed, and the impedance of the IM-MS interface. In configuration **C** the impedance of the skimmer-ion guide is proportional to the length of the ion-guide and to the inner diameter of the skimmer and ion-guide electrodes (Figure 1). The field strength in the ion-guide can be applied in numerous ways, analogous to previously reported IM cell designs (e.g., uniform or periodic).[31,32,41] The configuration described in this paper consists of ring electrodes distributed along the IM axis in a 3:5 spacing ratio, with the same voltage drop applied between each electrode, which creates an alternating high-low field strength configuration (E_H:E_L) between subsequent electrodes (see region 2 of Figure 1). The high-low field strength is related as $E_L = 0.6E_H$, where $E_H = \Delta V/l \times n$, ΔV is the total voltage drop across region 2, n is the number of electrodes in the ion guide, and l is the shortest electrode spacing distance.

Ion trajectory simulations were used to illustrate the influence of the pressure gradient (number of collisions) and applied field strength (relative ion−neutral velocities) on the ion heating process (T_{eff}) in the stacked-ring ion guide IM-MS interface. For example, the number of collisions, the ion kinetic energy, and the T_{eff} of ions as they traverse the IM-MS interface under low field strength values across region 2 (E_H = 40 V/cm) are contained in Figure 3a. The average T_{eff} and ion kinetic energy (red line) oscillate as a consequence of a E_H:E_L field strength configuration of the ion guide electrode design of region 2. Although the E_H and E_L values are constant, there is a pressure drop in region 2, that is, the E/P ratio is increasing. The increase in E/P causes the number of collisions/mm to decrease and the ion kinetic energy to increase toward the end of region 2. As a result, a larger kinetic energy is transferred into internal energies toward the end of region 2 ($T_{eff} \propto \Delta KE$), that is, the average T_{eff} increases as the ions drift in region 2. Although only a small increase in T_{eff} is observed at E_H = 40 V/cm, when the field strength in region 2 is increased to a higher value (E_H = 150 V/cm), a gradual ion heating is observed as depicted in the larger T_{eff} values illustrated in Figure 3b. This simulation shows that a stacked-ring ion guide design is well-suited for controlled ion heating (collisional activation) in the IM-MS interface because (i) the number of collisions can be controlled by the pressure drop (length of the ion guide), and (ii) the collision energy can be tuned by adjusting the field strength (E_H). It is important to note that the kinetic energy distribution of precursor and fragment ions exiting region 2 does not compromise the TOF resolving power, that is, the fraction of ion kinetic energies derived from the collisional activation/dissociation is small relative to that provided by the beam shaping and steering lenses.

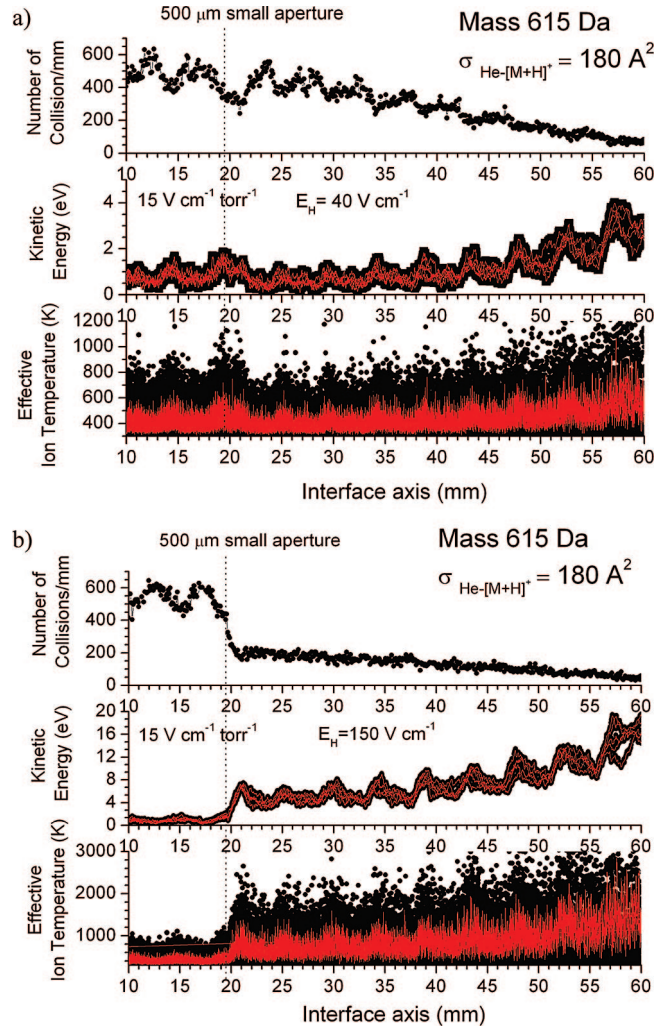

Figure 3. Simulations of the ion dynamics in the CID interface (configuration **C**). The dots represent single ion-neutral collisions, and the red lines the average for several ion trajectories. The numbers of collision/mm, the kinetic energy (eV), and the effective ion temperature (K) are illustrated for the "no CID" (a) and "CID" regime (b) for a singly charged model molecule of 615 Da mass and 180 Å^2 ion-neutral collision cross section ion ($\sigma_{He\text{-}[M+H]^+}$), equivalent values to those expected for a $[M + H]^+$ peptide such as RVGVAGG, VGVRAGG, and VGVAGGR. The field strength in the IM cell is 15 V cm^{-1} torr^{-1} and in the CID region are E_H = 40 V/cm and E_H = 150 V/cm for the "no CID" and "CID" regime, respectively.

In fact, as a consequence of the multicollisional nature of the ion activation/deactivation process in region 2, this experiment shares similarities with previously reported activation methods in radio frequency ion trap and Fourier transform − ion cyclotron resonance mass spectrometers, for example, (i) collisional activation in radio frequency ion trap [57−59] and sustained "off-resonance" irradiation (SORI) collisionally activated dissociation (CAD),[60−62] (ii) blackbody infrared dissociation (BIRD),[63] and infrared mul-

(55) Price, P. C.; Swofford, H. S.; Buttrill, S. E. *Anal. Chem.* **1977**, *49*, 1497–1500.
(56) Blom, K.; Munson, B. *J. Am. Chem. Soc.* **1983**, *105*, 3793–3799.
(57) Gronert, S. *J. Am. Soc. Mass Spectrom.* **1998**, *9*, 845–848.
(58) Goeringer, D. E.; Duckworth, D. C.; McLuckey, S. A. *J. Phys. Chem. A* **2001**, *105*, 1882–1889.
(59) Tolmachev, A. V.; Vilkov, A. N.; Bogdanov, B.; Pasa-Tolic, L.; Masselon, C. D.; Smith, R. D. *J. Am. Soc. Mass Spectrom.* **2004**, *15*, 1616–1628.
(60) Gauthier, J. W.; Trautman, T. R.; Jacobson, D. B. *Anal. Chim. Acta* **1991**, *246*, 211–225.
(61) Laskin, J.; Futrell, J. H. *Mass Spectrom. Rev.* **2005**, *24*, 135–167.
(62) Boering, K. A.; Rolfe, J.; Brauman, J. I. *Int. J. Mass Spectrom. Ion Processes* **1992**, *117*, 357–386.

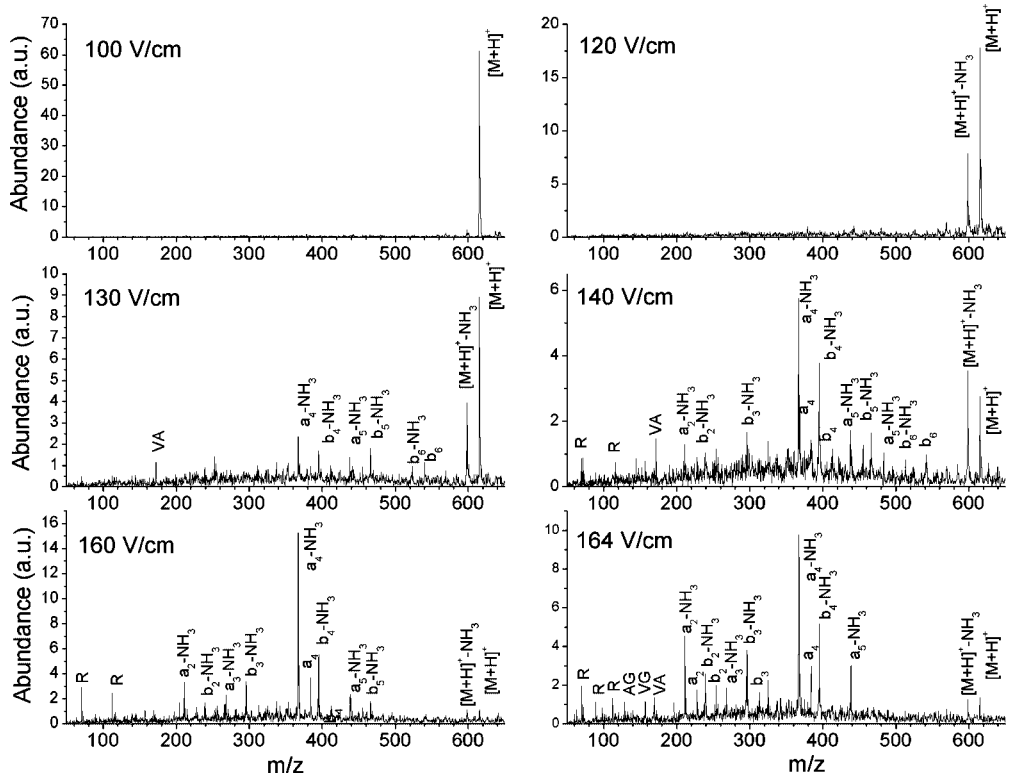

Figure 4. MALDI-IM-CID-oTOF fragmentation spectra of the RVGVAGG ($[M + H]^+$) peptide ion at different field strengths in region 2 (E_H = 100−164 V/cm).

tiphoton dissociation (IRMPD).[64] All of these techniques involve a periodic ion heating mechanism prior to ion dissociation. In our case, as a consequence of the E_H/E_L field strength configuration, ions are heated/cooled as they drift in region 2, whereas in the previously mentioned techniques the ion heating/cooling occurs by (i) ion excitation using a waveform in which ions are continuously undergoing accelerating/decelerating cycles, or (ii) IR photon absorption/radiative emission cycles. Although the activation time scale in our experiment (~10−100 μs) is shorter than those previously mentioned, a low energy rearrangement with decomposition occurring by the lowest energy pathway is the most probable dissociation mechanism. That is, the slow ion-heating by multiple, low energy collisions increases the fragmentation efficiency of the lower energy dissociation channels.

The variation of the relative abundances in the fragment ion spectra as a consequence of the activation process that occurs in region 2 when the field strength is increased (E_H = 100−164 V/cm) is illustrated in Figure 4 for a model peptide ion (RVGVAGG, $[M + H]^+$). At lower field strengths (E_H up to 100 V/cm), region 2 transfers the ions into the TOF ion source without fragmentation (as shown in Figure 4a). As the field strength increases (E_H = 100−164 V/cm) fragment ions are observed, where the fragment ion population varies from a high abundance of high m/z fragment ions to a high abundance of low m/z fragment ions with the field strength increase. The first dissociation channel observed is the neutral loss of NH_3 through the reaction $[M + H]^+ \rightarrow [M - NH_3 + H]^+ + NH_3$. Higher energy dissociation channels showed a neutral loss of NH_3 for the most abundant fragment ions. These results agree with the simulation shown in Figure 3, that is, at low field strength ions are transmitted into the TOF ion source and, as the field strength is increased, the collisional activation thresholds of higher energy dissociation channels are achieved.

The low-energy, multicollision nature of the activation process in region 2 suggests that dissociation occurs through the lowest energy dissociation channels, and with the field strength increase, higher energy dissociation channels become energetically accessible. To obtain a better description of the RVGVAGG ($[M + H]^+$) parent and fragment ion dissociation pattern, MS^n experiments using a ThermoFinnigan LCQ Deca Mass Spectrometer (San Jose, CA) were also performed. In the MS^n experiments, m/z ions of interest are isolated and further subjected to collisional activation until the first dissociation channel is observed. For the RVGVAGG ($[M + H]^+$) ions, the MS^n experiments were performed until the lowest m/z fragment ions were observed (in this case, arginine immonium ions), and the results are summarized in the scheme contained in Figure 5. The first and lowest energy dissociation channel is the neutral loss of NH_3 from the $[M + H]^+$ parent ion, in good agreement with the IM-CID-MS results contained in Figure 4 and previous BIRD experiments.[63] Subsequent fragmentation of the $[M - NH_3 + H]^+$ ion leads to the observation of b_i - NH_3 and a_i - NH_3 type ions (MS^3). Fragmentation of b_i - NH_3 and a_i - NH_3 ions leads to the observation a_i - NH_3 and b_{i-1} - NH_3 ions (MS^4), respectively. This pattern continues until the observation of arginine immonium ions. The MS^n dissociation scheme of

(63) Schnier, P. D.; Price, W. D.; Jockusch, R. A.; Williams, E. R. *J. Am. Chem. Soc.* **1996**, *118*, 7178–7189.
(64) Bomse, D. S.; Woodin, R. L.; Beauchamp, J. L. *J. Am. Chem. Soc.* **1979**, *101*, 5503–5512.

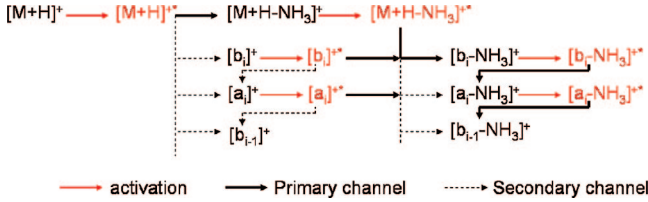

Figure 5. Ion fragmentation MS^n scheme observed for the RVGVAGG ($[M + H]^+$) peptide ion.

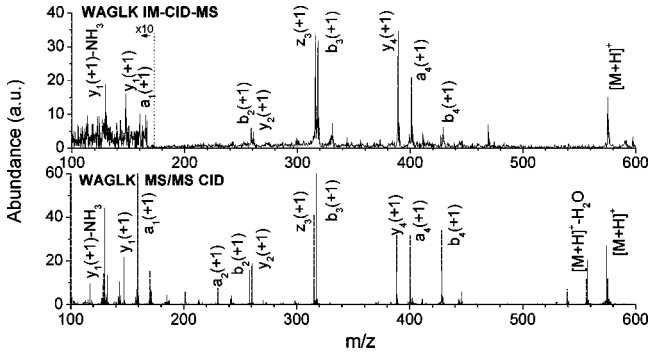

Figure 6. (a) MALDI-IM-CID-oTOF and (b) MALDI-MS/MS CID spectra of the WAGLK ($[M + H]^+$) peptide ion.

the RVGVAGG ($[M + H]^+$) ions is consistent with the low-energy, multicollisional nature of the CID observed in region 2, that is, the variation from a high abundance of high m/z fragment ions to a high abundance of low m/z fragment ions as the field strength is increased is a consequence of the sequential fragmentation pattern of the RVGVAGG ($[M + H]^+$) ion as depicted in Figure 5.

Fragmentation of RVGVAGG $[M + H]^+$ ions at higher collision energies yields b_i and a_i type ions (MS^2). Subsequent fragmentation of the b_i - and a_i - type ions shows the neutral loss of NH_3 as the lowest energy channel (MS^3), and at higher energies the observation of a_i - and b_{i-1} - type ions (MS^3), respectively. As a result, most of the fragmentation channels lead to the observation of fragment ions with the neutral loss of NH_3. This is in agreement with the trend observed in the IM-CID-MS experiment, as shown in Figure 4. That is, the neutral loss of NH_3 for *a*- and *b*- fragment ions is the lowest energy and first observed dissociation channel, which is exemplified by the large abundance of fragment ions with a loss of NH_3 in the IM-CID-MS spectra contained in Figure 4.

The collisional activation of other R containing peptides (e.g., RGG, GRG, GGR, VGVRAGG, and VGVAGGR peptides - see Supporting Information) also share the neutral loss of NH_3 from the $[M + H]^+$ parent ion as the first and lowest energy dissociation channel (Figure 5). Peptides that do not contain R, however, do not show the neutral loss of NH_3 as the more abundant dissociation channels. This is illustrated in the example of Figure 6a, where a IM-CID-MS spectrum for WAGLK ($[M + H]^+$) peptide ion is contained. The CID spectrum consists primarily of *a*-, *b*-, and *y*− type fragment ions and no neutral loss of NH_3 is observed. The high abundance of fragment ions observed in the CID spectra using the stacked-ring ion guide design for the IM-CID-MS permits an accurate identification of the parent ion, which makes this instrument a good candidate for the analysis of biological samples. Notice

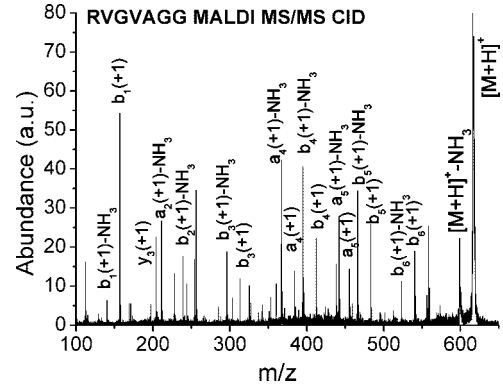

Figure 7. MALDI-MS/MS CID spectrum for the RVGVAGG ($[M + H]^+$) peptide ion.

that in the case of IM-CID-MS, as we mentioned before, the CID is performed concurrently since the parent ions are already separated in the IM domain, unlike in other tandem MS experiments where the masses of the parent ions must be selected individually. That is, the IM-CID-MS is a feasible tool for analyses of complex samples because of its large throughput and the relatively short time scale on which the analysis is performed.

In addition, to evaluate the applicability of the stacked-ring ion guide of the IM-CID-MS for routine peptide characterization, the IM-CID-MS fragmentation was compared to that of the MALDI MS/MS CID, which is commonly used in routine MS/MS analysis of biological samples. The MALDI MS/MS CID was performed in an Applied Biosystems 4700 Mass Spectrometer (Framingham, MA). In the MALDI MS/MS CID, the fragmentation spectra show similar features to those observed in the IM-CID-MS: a large abundance of *a*-, *b*-, and *y*− type ions with neutral loss of NH_3 for the R-containing peptides (Figures 6b and 7). The similarities of the MALDI MS/MS CID and IM-CID-MS data may be attributed to the multicollisional nature of the CID process.[65]

CONCLUSIONS

The use of a stacked-ring ion guide and pressure gradient configuration as an IM-MS interface to study the collisional activation and the lowest energy dissociation pathway of ions exiting the IM drift cell is described. The T_{eff} extracted from the ion dynamic simulations provides a good description of the physical processes that occur during the ion heating mechanism as a consequence of *E/P* ratio increase as the ions drift in region 2. The collisional activation and low energy, multicollisional nature of the IM-CID-MS was verified with fragmentation studies of a series of model peptide ions. The high abundance of fragment ions observed in the CID spectra using the stacked-ring ion guide design for the IM-CID-MS permits an accurate identification of the parent ion, which makes this instrument a good candidate for the analysis of biological samples. The stacked-ring ion guide design for the IM-MS interface shows good transmission of IM separated ions to the MS source at low field strength ($T_{eff} \sim T_{BG}$), and as field strength is increased ($T_{eff} > T_{BG}$), can be employed to perform collisional activation leading to rearrangement reactions and/or fragmentation.

(65) Cotter, R. J.; Griffith, W.; Jelinek, C. *J. Chromatogr. B* **2007**, *855*, 2–13.

The characterization of a molecule on the basis of mobility or collision cross-section, mass-to-charge ratio, and tunable fragmentation pattern in a single apparatus is a feasible tool for analyses of complex samples owing to its large throughput and the relatively short time scale on which MALDI-IM-CID-MS experiments can be conducted when compared with traditional MALDI-MS/MS CID methodology. In a separate paper, the applicability of the IM-MS interface for the analysis of complex biological mixtures (e.g., higher molecular weight model peptide ions and protein digest) will be discussed.[66]

ACKNOWLEDGMENT

This work was supported by the Robert A. Welch Foundation (A-1176) and the U.S. Department of Energy, Division of Chemical Sciences, BES (DE-FG-04ER-15520) grants. We acknowledge the helpful discussion and guidance of the Prof. Angela Nickele with the gas simulations using the Fluent Inc. software. We appreciate the assistance of Dr. J. G. Slaton in the peptide synthesis. We also acknowledge the helpful discussion with our colleagues from Ionwerks Inc.

(66) Becker, C.; Fernández-Lima, F. A.; Gillig, K. J.; Russell, W. K.; Cologna, S.; Russell, D. H. *J. Am. Soc. Mass Spectrom.* **2008**, in press.

SUPPORTING INFORMATION AVAILABLE

Typical fragmentation spectra of several model peptide ions obtained using the IM-CID-MS configuration. This material is available free of charge via the Internet at http://pubs.acs.org.

Received for review September 9, 2008. Accepted November 7, 2008.

AC801919N